International Journal of Research in Science and Technology
Volume 10, Issue 1: January - March 2023

ISSN 2394 - 9554

AN APPROACH TO REDUCE THE COMPUTATIONAL STEPS OF PREDICTIVE CURRENT CONTROLLER WITH CONSTANT SWITCHING FREQUENCY IN DISTRIBUTION SYSTEMS HAVING FOUR-LEG PHOTOVOLTAIC INVERTER

Joe Brislin and Sundaram Maruthachalam
Department of Electrical and Electronics Engineering, PSG College of Technology, Coimbatore, India

ABSTRACT

Distribution systems with renewable energy sources require a neutral terminal connection between the load and inverter. This can be provided by a four-leg voltage source inverter that suppresses zero sequence harmonics when a non-linear or unbalanced load is used. Various conventional control techniques are available for current control in four-leg inverters. Among them, model predictive control shows promising performance with less control complexity. The model predictive current control has limitations in practical implementation due to the nature of its varying switching frequency and its impact in filter design. Hence a modulator is used to overcome this limitation. The modulated model predictive current control combines the advantages of predictive control like quick transient response and linear control of space vector modulation. The control objective is to optimize the modulation time ratio rather than the switching states using a cost function and thus obtain a constant switching frequency. The proposed approach aims to reduce the computational steps involved in the modulation stage. This is done by incorporating the activation order of the active voltage vectors which are calculated using simple formulas and only one look-up table. As very low value of sampling time is taken, extrapolation is avoided in the predictive model and in turn reduces the computational burden substantially. The calculations are done in one sampling period and the switching states are applied in the next instant. The performance of the same is validated through simulation carried in MATLAB/Simulink environment. Level 2 S-Function block which uses C code is used for simulation as it can accommodate discrete system and it can also be used in device drivers during hardware implementation.

Keywords— Four-leg inverter, Predictive current control, Shunt active power filter, Standalone hybrid power system, S-function, Three-dimensional space vector modulation.

I. INTRODUCTION

As renewable sources are proven to be the cleanest source of energy, ample measures are being taken to integrate the same with the distributed generation systems. Integrating the renewable sources to the grid comes with its own challenges in addition to the issues caused by load side fluctuations. Increasing the level of voltage source inverters in renewable source application leads to increase in number of switches, sensors and thus leads to complex control techniques [1]. By adding an extra leg to the conventional three-leg inverters, most of the problems arising due to unbalanced or non-linear loads can be managed. The midpoint from the fourth leg containing two switches is connected to the neutral point of the load [2]. This topological modification gives numerous advantages including flexibility in control, output voltage/current quality improvement [3].

Many applications like active front end rectifiers, hybrid distribution generation systems, shunt active power filter and electric drives can utilize the potential of current control technique in four-leg inverter [4]. Considering the non-linear characteristic nature of renewable energy sources and consequently its effect on power distribution system, a robust compensation system like a shunt active power filter having a four-leg photovoltaic inverter can be used [2]. One typical example of utilising a four-leg photovoltaic inverter as shunt active power filter in standalone power system having hybrid source of energy is presented in Fig 1.

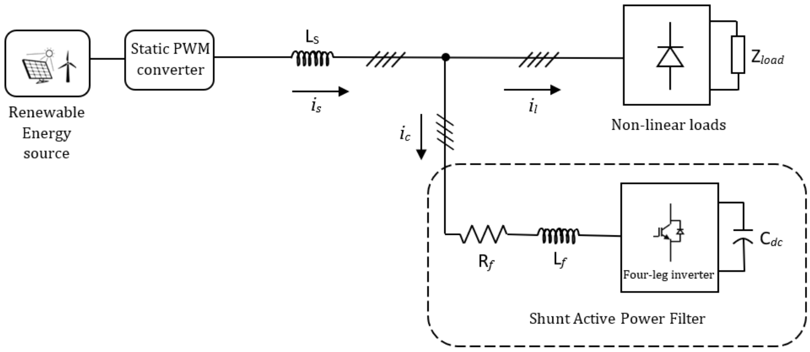

Fig 1: Configuration of Standalone power system with renewable source, SAPF and four-leg photovoltaic inverter

ISSN 2394 - 9554

The conventional techniques to control current for a four-leg photovoltaic inverter use PID regulators followed by a duty ratio modulator to generate the gating signals [4]. Three dimensional space vector modulation is also touted to be a very comprehensible control technique for four leg inverters as it has numerous advantages of dc-link utilization and minimal distortion in output [6]. Comparatively, Model predictive current control is quite an attractive control method when compared to the conventional control techniques. It shows promising effects by having fast dynamic response, robustness in adapting to the reference current, preserving a constant DC link voltage and including non-linearities while designing the discrete model of the system [7]. The only drawback faced is the variable switching frequency during operation. This leads to complication in the filter design as the filter gets bulky for a wide spectrum of harmonics [8].

By blending the advantages from both the conventional and model predictive current control together, the time interval for the switching sequence is calculated by introducing a modulator in between the control circuit and power circuit [9]. Though a modulator is present, the inner current control loop is completely avoided as predictive control does its work in the discrete model of the system using finite control set. As its name, this control technique predicts the output current of the next sampling instant and uses it to generate the required switching sequence. The switching sequence is then sent through a modulator, so that an optimized set of switching signal with constant frequency can be obtained [10].

The working of the proposed control scheme is validated by the simulations done in Simulink, Matlab. The same has been validated for various source and load conditions. This paper is organised as following sections: In Section II, the discrete-time model of the system is derived along with the mathematical explanation of the four-leg inverter topology. In Section III, the proposed control strategy with reduced computation steps is discussed along with their conventional counterparts. In Section IV, simulation results are presented and inferred followed by appropriate conclusion in Section V.

II. SYSTEM DESCRIPTION AND MODELLING OF FOUR-LEG VOLTAGE SOURCE INVERTER

A. Topology

Fig 2 shows the topology of the two-level four-leg photovoltaic inverter with voltage-source and non-linear load. R_{fa}, R_{fb}, R_{fc}, R_{fn} represent the leakage resistance of the filter. L_{fa}, L_{fb}, L_{fc}, L_{fn} represent the filter inductance. R_{fn} and L_{fn} facilitates the controllability of the zero-sequence current. R_a, R_b and R_c are taken as the load resistances.

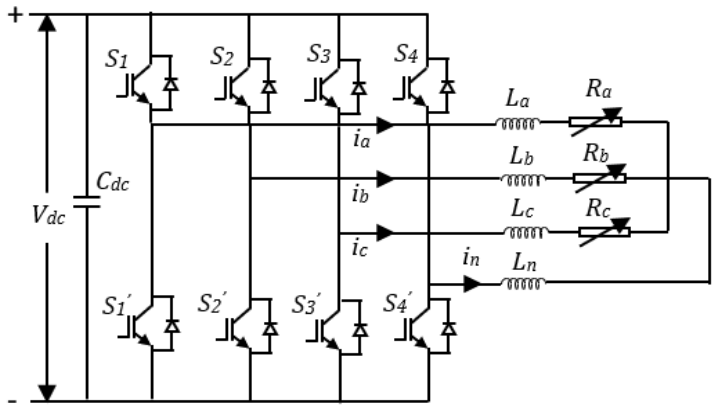

Fig 2: Topology of typical Four-leg Photovoltaic Inverter having Voltage Source

Although the presence of additional leg in the inverter increases the complexity of the control, it can be used to handle balanced or unbalanced, linear or non-linear, and single or three-phase loads without having an impact on the dc-link capacitor. i_a, i_b, i_c, and i_n are the output load currents [8].

B. Mathematical Model

Due to the topology, four switching signals S_1, S_2, S_3, S_4 are required and it leads to a total of 16 (2^4) switching states. The instantaneous output voltages across the load of the four-leg inverter [7] can be expressed as in (1)

$$V_{gN} = R_{fg} i_g + L_{fg} \frac{di_g}{dt} + V_{nN}, \quad g = a, b, c, n \tag{1}$$

The output load voltages of the inverter in terms of its load parameters can be expressed as in (2)

$$\begin{bmatrix} V_{an} \\ V_{bn} \\ V_{cn} \end{bmatrix} = R_{eq} \begin{bmatrix} i_a \\ i_b \\ i_c \end{bmatrix} + L_{eq} \frac{d}{dt} \begin{bmatrix} i_a \\ i_b \\ i_c \end{bmatrix} \tag{2}$$

Where,

$$R_{eq} = \begin{bmatrix} R_a + R_{fa} + R_{fn} & R_{fn} & R_{fn} \\ R_{fn} & R_b + R_{fb} + R_{fn} & R_{fn} \\ R_{fn} & R_{fn} & R_c + R_{fc} + R_{fn} \end{bmatrix}$$

and

$$L_{eq} = \begin{bmatrix} L_{fa} + L_{fn} & L_{fn} & L_{fn} \\ L_{fn} & L_{fb} + L_{fn} & L_{fn} \\ L_{fn} & L_{fn} & L_{fc} + L_{fn} \end{bmatrix}$$

The change in output current can be expressed from (1) as

$$\frac{di_g}{dt} = \frac{1}{L_{fg}}\left[\left(V_{gN} - V_{nN}\right) - R_{fg} i_g\right], \qquad g = a, b, c, n \tag{3}$$

From (2), the load current in continuous time-domain can be expressed as

$$\frac{d}{dt}\begin{bmatrix} i_a \\ i_b \\ i_c \end{bmatrix} = A \begin{bmatrix} i_a \\ i_b \\ i_c \end{bmatrix} + B \begin{bmatrix} V_{an} \\ V_{bn} \\ V_{cn} \end{bmatrix} \tag{4}$$

Where

$$A = L_{eq}^{-1} R_{eq}, \qquad B = L_{eq}^{-1}$$

III. Improved Modulated MPCC with Reduced Computations

The block diagram of the Improved Modulated MPCC for a three-phase four-leg photovoltaic inverter [9] having resistive (R) load is shown in Fig 3. For easy understanding, the conventional MPCC and MPCC with constant switching frequency are discussed first followed by the improved method of Modulated MPCC with reduced computations.

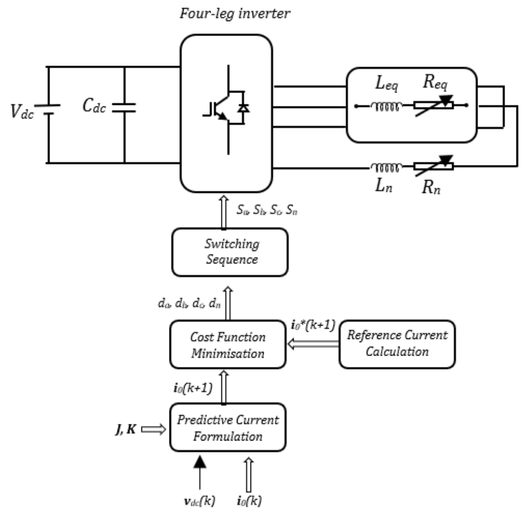

Fig 3: Block Diagram of Improved Modulated MPCC of four-leg Photovoltaic Inverter

A. Conventional Model Predictive Current Control (MPCC)

For the design process and digital implementation, the load currents in state-space representation and discrete-time model is required. The voltage applied at the output RL filter can be written as shown in (5)

$$\begin{bmatrix} V_{an} \\ V_{bn} \\ V_{cn} \end{bmatrix} = \begin{bmatrix} S_1 - S_4 \\ S_2 - S_4 \\ S_3 - S_4 \end{bmatrix} V_{dc} \tag{5}$$

The design procedure of the conventional Model Predictive Current control are as follows.

Step 1. Required Measurements

The output load current and voltage across DC-link capactitor are the required input components of the feedback system. For this, three current sensor across each phase and one voltage sensor across DC-link capacitor is required. The output load voltage in terms of DC-link voltage and switching signals can be easily calculated from (4).

Step 2. Generation and Extrapolation of Reference currents
The future prediction of load current reference is calculated using fourth-order Lagrange extrapolation. The fourth-order is utilized for a broad range of frequencies of reference output current, i*. The calculation of future load current is done as follows.

$$i^*[k+1] = 4i^*[k] - 6i^*[k-1] + 4i^*[k-2] - i^*[k-3] \quad (6)$$

Step 3. Formulation of Predictive Load currents
The formulation of predictive load currents is done by considering both the converter and load in the discrete-time domain. Additional constraints like sampling time and approximations can be included in the models. A recursive matrix equation is derived for the discrete-time model and it calculates the system prediction. The system states at any instant $(k+1)T_s$ for a given sampling time, T_s can be predicted with the feedback components known at instant $(k)T_s$. The recursive equation is formulated as shown in (7)

$$i[k+n+1] = \mathbf{Ji}[k+n] + \mathbf{Kv}[k+n] \quad (7)$$

Where

$$J = \begin{bmatrix} j_1 & j_2 & j_3 \\ j_4 & j_5 & j_6 \\ j_7 & j_8 & j_9 \end{bmatrix} = e^{AT_s}$$

$$K = \begin{bmatrix} k_1 & k_2 & k_3 \\ k_4 & k_5 & k_6 \\ k_7 & k_8 & k_9 \end{bmatrix} = A^{-1}(J - I_{3x3})B$$

Since matrices of order 3 are involved, to reduce the computation for every sampling instant, the values are calculated offline and then used in prediction algorithm.

Step 4. Estimation of Cost Function
The space vector diagram of four-leg inverter contains 6 prisms with 4 tetrahedrons each. So, 24 tetrahedrons are present that enclose 16 switching vectors of the photovoltaic inverter. Each tetrahedron has 3 active voltage vectors. The active voltage vectors are V_1 to V_{14} and produce non-zero output voltage. V_0 and V_{15} are the zero-voltage vectors and they produce no output voltage. By selecting them appropriately in a switching sequence, the switching frequency can be reduced. The switching states along with their corresponding voltage vectors are highlighted in Table 1. With 16 (24) combination of the switching signals, 16 predictions of the load current are obtained.

Table 1: Voltage Vectors and Switching States for Four-Leg Photovoltaic Inverter

V	c	S_1	S_2	S_3	S_4
V_0	c_0	0	0	0	0
V_1	c_1	0	0	1	0
V_2	c_2	0	1	0	0
V_3	c_3	0	1	1	0
V_4	c_4	1	0	0	0
V_5	c_5	1	0	1	0
V_6	c_6	1	1	0	0
V_7	c_7	1	1	1	0
V_8	c_8	0	0	0	1
V_9	c_9	0	0	1	1
V_{10}	c_{10}	0	1	0	1
V_{11}	c_{11}	0	1	1	1
V_{12}	c_{12}	1	0	0	1
V_{13}	c_{13}	1	0	1	1
V_{14}	c_{14}	1	1	0	1
V_{15}	c_{15}	1	1	1	1

The control objective of the predictive current control is achieved by formulating the cost function. The 16 predictions for i[k+1] are found using (7) and then compared with their respective reference currents. The comparison yields the cost function value. Cost function, c is found as follows

$$c[k+1] = (i_a^*[k+1] - i_a[k+1])^2 + (i_b^*[k+1] - i_b[k+1])^2 + (i_c^*[k+1] - i_c[k+1])^2 \tag{8}$$

$$c[k+1] = ||i^*[k+1] - i[k+1]||^2 \tag{9}$$

The formulation in (8) leads to 16 different cost function values pertaining to the 16 voltage vectors in Table 1. The real work of minimal cost function block is to gather the minimum value of cost function and identify its corresponding switching state. For example, if cost function c_5 has a minimal value among the calculated values of c_0 to c_{15}, the switching state combination corresponding to c_5 is taken as the optimum choice and applied directly to the four-leg inverter. The conventional predictive current control does not have a modulating stage and it causes variable switching frequency during implementation.

B. MPCC WITH CONSTANT SWITCHING FREQUENCY

Step 5. Calculation of Modulation Time Ratio

The constant switching frequency can be obtained in Predictive Current Control by adding a modulator. The control objective of the controller now shifts from optimizing the switching states to optimizing the modulation time ratio. For this, 3 active voltage vectors and 1 zero-voltage vector (V_i, V_j, V_k and V_0) and their corresponding cost function values (c_i, c_j, c_k and c_0). The relationship between Voltage vectors, duty cycle and the cost function are tabulated exhaustively in Table 2.

Table 2: Adjacent Voltage Vectors, Duty Cycles and Cost Functions in the 24 Tetrahedrons (T) of a Four-Leg Photovoltaic Inverter

T	**W**	**V_0**	**V_i**	**V_j**	**V_k**	**d_0**	**d_i**	**d_j**	**d_k**	**c_0**	**c_i**	**c_j**	**c_k**
1	W_0	V_0	V_4	V_{12}	V_{14}	d_0	d_4	d_{12}	d_{14}	c_0	c_4	c_{12}	c_{14}
2	W_1	V_0	V_4	V_6	V_{14}	d_0	d_4	d_6	d_{14}	c_0	c_4	c_6	c_{14}
3	W_2	V_0	V_4	V_6	V_7	d_0	d_4	d_6	d_7	c_0	c_4	c_6	c_7
4	W_3	V_0	V_8	V_{12}	V_{14}	d_0	d_8	d_{12}	d_{14}	c_0	c_8	c_{12}	c_{14}
5	W_4	V_0	V_3	V_6	V_{14}	d_0	d_3	d_6	d_{14}	c_0	c_3	c_6	c_{14}
6	W_5	V_0	V_3	V_{10}	V_{14}	d_0	d_3	d_{10}	d_{14}	c_0	c_3	c_{10}	c_{14}
7	W_6	V_0	V_3	V_6	V_7	d_0	d_3	d_6	d_7	c_0	c_3	c_6	c_7
8	W_7	V_0	V_8	V_{10}	V_{14}	d_0	d_8	d_{10}	d_{14}	c_0	c_8	c_{10}	c_{14}
9	W_8	V_0	V_3	V_{10}	V_{11}	d_0	d_3	d_{10}	d_{11}	c_0	c_3	c_{10}	c_{11}
10	W_9	V_0	V_3	V_3	V_{11}	d_0	d_3	d_3	d_{11}	c_0	c_3	c_3	c_{11}
11	W_{10}	V_0	V_3	V_3	V_7	d_0	d_3	d_3	d_7	c_0	c_3	c_3	c_7
12	W_{11}	V_0	V_8	V_{10}	V_{11}	d_0	d_8	d_{10}	d_{11}	c_0	c_8	c_{10}	c_{11}
13	W_{12}	V_0	V_1	V_3	V_{11}	d_0	d_1	d_3	d_{11}	c_0	c_1	c_3	c_{11}
14	W_{13}	V_0	V_1	V_9	V_{11}	d_0	d_1	d_9	d_{11}	c_0	c_1	c_9	c_{11}
15	W_{14}	V_0	V_1	V_3	V_7	d_0	d_1	d_3	d_7	c_0	c_1	c_3	c_7
16	W_{15}	V_0	V_8	V_9	V_{11}	d_0	d_8	d_9	d_{11}	c_0	c_8	c_9	c_{11}
17	W_{16}	V_0	V_1	V_9	V_{13}	d_0	d_1	d_9	d_{13}	c_0	c_1	c_9	c_{13}
18	W_{17}	V_0	V_1	V_5	V_{13}	d_0	d_1	d_5	d_{13}	c_0	c_1	c_5	c_{13}
19	W_{18}	V_0	V_1	V_5	V_7	d_0	d_1	d_5	d_7	c_0	c_1	c_5	c_7
20	W_{19}	V_0	V_8	V_9	V_{13}	d_0	d_8	d_9	d_{13}	c_0	c_8	c_9	c_{13}
21	W_{20}	V_0	V_4	V_5	V_{13}	d_0	d_4	d_5	d_{13}	c_0	c_4	c_5	c_{13}
22	W_{21}	V_0	V_4	V_{12}	V_{13}	d_0	d_4	d_{12}	d_{13}	c_0	c_4	c_{12}	c_{13}
23	W_{22}	V_0	V_4	V_5	V_7	d_0	d_4	d_5	d_7	c_0	c_4	c_5	c_7
24	W_{23}	V_0	V_8	V_{12}	V_{13}	d_0	d_8	d_{12}	d_{13}	c_0	c_8	c_{12}	c_{13}

The sixteen cost function values listed in Table 1 are used to determine the modulation ration for the stationary voltage vectors as follows

$$d_i = \frac{c_j c_k c_0}{c_i c_j c_k + c_j c_k c_0 + c_i c_j c_0 + c_i c_k c_0}$$

 ISSN 2394 - 9554

$$d_j = \frac{c_j c_k c_0}{c_i c_j c_k + c_j c_k c_0 + c_i c_j c_0 + c_i c_k c_0}$$

$$d_k = \frac{c_i c_j c_0}{c_i c_j c_k + c_j c_k c_0 + c_i c_j c_0 + c_i c_k c_0}$$

$$d_0 = \frac{c_j c_j c_k}{c_i c_j c_k + c_j c_k c_0 + c_i c_j c_0 + c_i c_k c_0}$$

Step 6. Selection of Switching Sequence

After calculating the modulation ratio of the space vectors, it is necessary to pick the appropriate switching sequence. The switching sequence has no effect on the output voltage but it has effect on the harmonic spectral content of the inverter output and power losses. Symmetrical switching sequence is selected as it has proper symmetry within the modulation time period and it consequently shapes the desired harmonic spectrum produced in the inverter output [11].

Step 7. Modified Cost Function

A modified cost function is used to calculate the error in load current in each tetrahedron of the photovoltaic inverter.

$$W(k) = d_i g_i + d_j g_j + d_k g_k + d_0 g_0 \tag{10}$$

After calculating 24 different cost function that optimizes duty-cycle (W_0 to W_{23}) as shown in Table 2, the optimal stationary voltage vectors and duty cycles corresponding to the minimal cost function W is selected and the appropriate switching sequence is applied [12].

C. Improved Modulated MPCC with Reduced Computations

The symmetrically aligned switching sequence pattern has both zero vectors V0 and V15 within the modulation period. A nine-step switching sequence is selected and the time duration of each leg switching time is calculated.

$$T_a = \Delta T_{sw}\left(\frac{d_0}{4}\right)$$

$$T_b = \Delta T_{sw}\left(T_a + \frac{d_i}{2}\right)$$

$$T_c = \Delta T_{sw}\left(T_b + \frac{d_j}{2}\right)$$

$$T_0 = \Delta T_{sw}\left(T_c + \frac{d_0}{2}\right)$$

The activating order of each time duration can be found from the selected active vectors. The calculation in reduces the computational steps involved. Also, in order to avoid overmodulation or discontinuous pulse width modulation, the active vectors can be projected on the αβ and a cylindrical boundary can be maintained by checking ($|v_{\alpha\beta0}{}^*| \leq V_{dc}$). The zero-sequence voltage obtained from the fourth leg can also be limited by setting a spherical boundary by checking

$\sqrt{2}|\, v_{\alpha\beta0}{}^{*}| + |v_0{}^{*}| \leq \sqrt{3}V_{dc}$.

IV. DISCUSSIONS AND SIMULATION STUDIES

The proposed system has been validated through a simulation study on four-leg photovoltaic inverter in MATLAB/Simulink environment with the parameters mentioned in Table 3. The simulation model uses level 2 S-function block for computation. The S-function block in written in C code and then compiled as MEX file. Since S-Function is a user defined block, it can accommodate discrete system. It instructs the mathematical engine on what to do during initialization, update, output and termination. This particular distinct quality of S-Function block is used to implement the prediction model of k+1 instant in kth instant.

At the same time, the switching states after modulator stage can be updated to the power converter switches. This compensates the delay developed during the modulation stage. It also eases the digital implementation and can be easily incorporated in hardware device drivers. The simulation result for the proposed system with unbalanced reference currents and loads are studied and validated. It is compared with the conventional predictive current control model and their THD components are also discussed.

Table 3: Parameters of the Simulated System

Symbol	Parameter	Values
V_{dc}	DC link voltage	590 V
C_{dc}	DC capacitor	1000 µF
L_f	Filter inductance	5 mH
R_f	Filter resistance	0.5 Ω
T_s	Sampling time	20 µs
f_0	Load frequency	50 Hz
R_a	Phase-a load resistance	50 Ω
R_b	Phase-b load resistance	50 Ω
R_c	Phase-c load resistance	50 Ω

A. Step change in Unbalanced Reference Currents and Loads

The reference currents are changed with a step change at t = $0.5f_0$ (load frequency) as shown in Fig 4. The performance of the conventional MPCC at switching frequency T_{sw} = 2.2 kHz and the improved modulated MPCC with switching frequency T_{sw} = 10 kHz is shown in Fig 4(a) and Fig 4(b). As the modified cost function optimizes the modulation time ratio, the switching frequency is taken as 10 kHz. There is no overshoot observed in the step change at 0.01 second. The load currents also show better tracking performance and high transient response. Neutral current is developed in the system due to the load current unbalance and it flows through the additional leg of the inverter. The inverter line-line voltage can also be observed to have two levels. The proposed system is compared with the conventional MPCC where the sampling time is taken as 20 µs which is slightly reduced than the normal value.

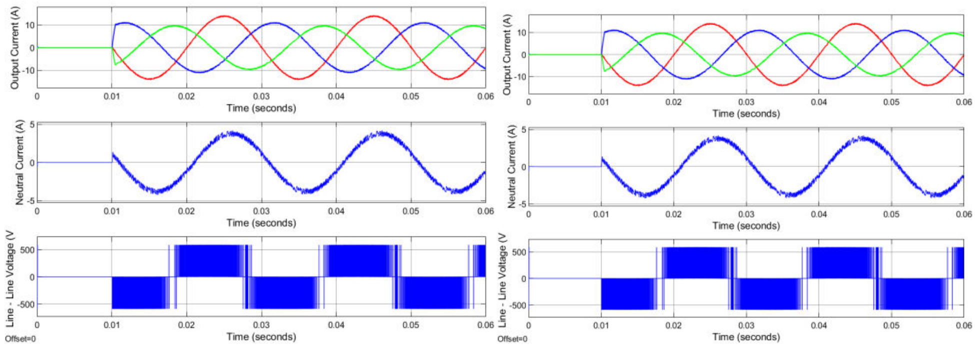

a) Conventional MPCC (F_{sw} = 2.2 kHz)

b) Improved Modulated MPCC (F_{sw} = 10 kHZ)

Fig 4 Simulation result for step change with unbalanced loads and reference currents: (i) Output current (A), (ii) Neutral current (A), (iii) Output line – line voltage (V)

The error in tracking is slightly observed as the optimal tetrahedron containing three active voltage vectors and zero voltage vector is selected during each sampling period rather than the optimized switching states. This happens because, the tetrahedron with three active voltage vectors are selected instead of one vector corresponding to the optimized switching state in conventional MPCC.

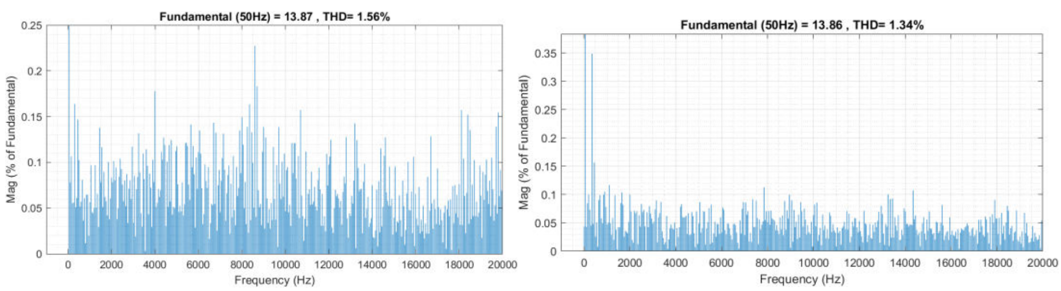

a) Conventional MPCC (F_{sw} = 2.2 kHz) and sampling time (Ts = 20 µs)

b) Improved Modulated MPCC (F_{sw} = 10 kHZ) and sampling time (Ts = 20 µs)

Fig 5 THD analysis on phase-b load current with unbalanced loads and reference currents

The THD analysis on phase-b load current is shown in Fig 5. Concentrated harmonics can be observed in Fig 5(b) at switching frequency, F_{sw} and its higher orders. This simplifies the process of designing a suitable filter for eliminating the harmonics content.

Considering the application of four-leg photovoltaic inverter in shunt active power filter for standalone hybrid power systems, the proposed scheme is tested for non-sinusoidal and trapezoidal reference currents as demonstrated in Fig 6. The loads are the same for both the conditions shown in Fig 6. For non-sinusoidal reference current, third order harmonic in injected. The simulation results show a good tracking capacity of the proposed system with a fast dynamic response. The neutral current discharges through the additional leg of the photovoltaic inverter due to non-sinusoidal reference currents.

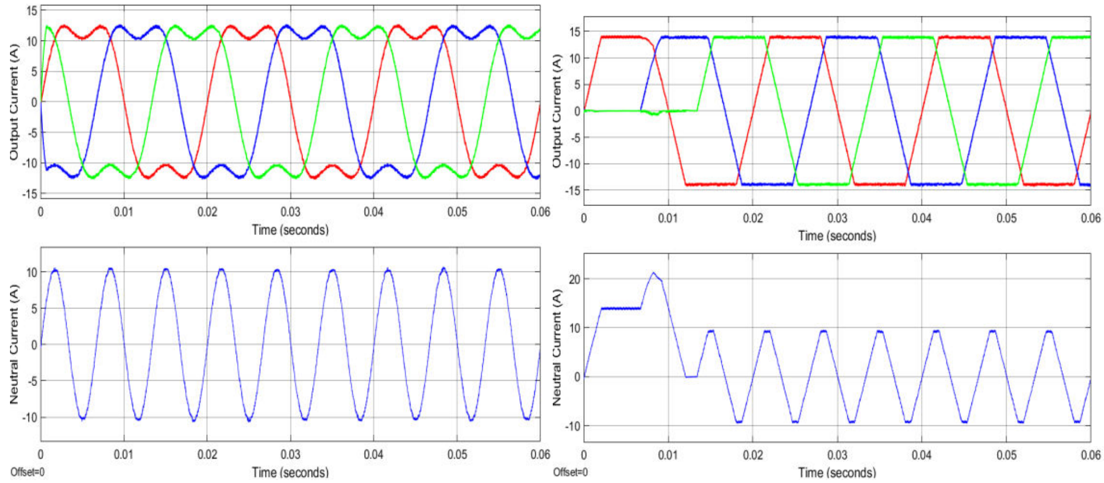

a) Non-sinusoidal reference currents

b) Trapezoidal reference currents

Fig 6 Simulation result of proposed system with non-sinusoidal and trapezoidal reference currents: (i) Output currents (A), (ii) Neutral current (A)

The simulation result of the proposed system with unbalanced and balanced reference current is shown in Fig 7. The optimal tetrahedron selection is also shown. It changes from 0 to 12 as balanced load is considered under steady-state. The simulation result of the proposed system ramp change in the balanced reference current is shown in Fig 8. The optimized tetrahedron is seen to change among 1 to 24 due to the ramp change in reference currents.

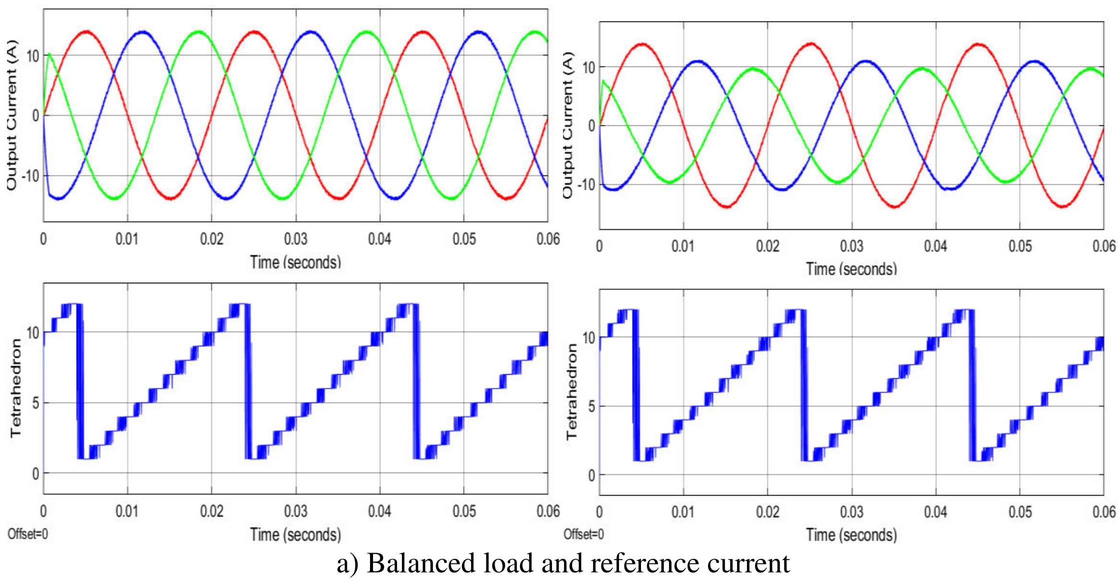

a) Balanced load and reference current

b) Unbalanced load and reference current

Fig 7 Simulation result with balanced and unbalanced loads and reference currents: (i) Output Current (A), (ii) Optimized tetrahedron selection

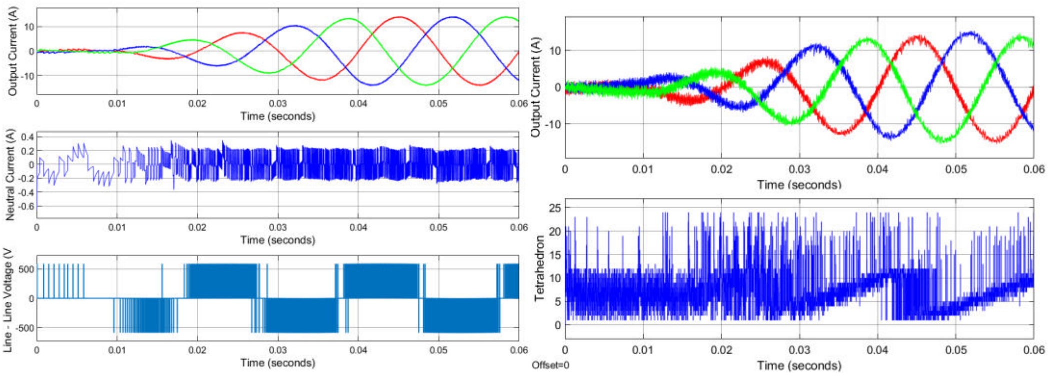

a) Ramp change in balanced reference current

b) Ramp change in in balanced reference current and unbalanced load condition

Fig 8 Simulation result with ramp change in unbalanced and balanced load conditions (i) Output Current (A), (ii) Optimized tetrahedron selection

CONCLUSION

An approach to reduce the number of computational steps in the modulated model predictive current control of the four-leg photovoltaic inverter is discussed in this paper. The proposed control strategy uses a cost function that optimizes the tetrahedron containing four voltage vectors and generate switching signals corresponding to the optimized tetrahedron. The operating principle from conventional MPCC and MPCC with constant switching frequency is combined and the computational steps of referring to the lookup table can be reduced by modifying the process of calculating the application interval from the optimized duty cycle values. A symmetrical type of switching sequence is selected as they limit the presence of harmonic content in higher frequencies. Most of the harmonic components are dominant around the constant switching frequency. The proposed system ensures fast dynamic response, low sampling rate due to reduced computational steps, low steady-state error and constant switching frequency.

REFERENCES

[1] J. Li, F. Zhuo, X. Wang, L. Wang, and S. Ni, "A grid-connected PV system with power quality improvement based on boost + dual-level four-leg inverter," in Proc. IEEE Int. Power Electron. and Motion Control Conf., Wuhan, China, May 2009, pp. 436–440.

[2] V. Yaramasu, M. Rivera, B. Wu and J. Rodriguez, "Model Predictive Current Control of Two-Level Four-Leg Inverters-Part I: Concept Algorithm and Simulation Analysis", IEEE Transactions of Power Electronics, vol. 28, no. 7, pp. 3459-3468, July 2013.

[3] P. Acuna, L. Moran, M. Rivera, J. Rodriguez and J. Dixon, "Improved active power filter performance for distribution systems with renewable generation", Proc. 38th Annu. Conf. IEEE Ind. Electron. Soc., pp. 1344-1349, Dec. 2012.

[4] M. Aredes, J. Hafner, and K. Heumann, "Three-phase four-wire shunt active filter control strategies," IEEE Trans. Power Electron., vol. 12, no. 2, pp. 311–318, Mar. 1997.

[5] X. Wei, "Study on digital pi control of current loop in active power filter," in Proc. 2010 Int. Conf. Electr. Control Eng., Jun. 2010, pp. 4287–4290

[6] Y R. Zhang, V. Prasad, D. Boroyevich and F. Lee, "Three-dimensional space vector modulation for four-leg voltage-source converters", IEEE Trans. Power Electron., vol. 17, no. 3, pp. 314-326, May. 2002.

[7] M. Rivera and V. Yaramasu, "Digital predictive current control of a three-phase four-leg inverter", IEEE Trans. Ind. Electron., vol. 60, no. 11, pp. 4903-4912, Nov. 2013

[8] V. Yaramasu, B. Wu, M. Rivera and J. Rodriguez, "Enhanced model predictive voltage control of four-leg inverters with switching frequency reduction for standalone power systems", Proc. EPE/PEMC, pp. DS2c.6-1-DS2c.6-5, Sep. 2012

[9] V. Yaramasu, K. Milev, A. Dekka, M. Rivera, J. Rodriguez and F. Rojas, "Modulated model predictive current control of a four-leg inverter", 2020 11th Power Electronics Drive Systems and Technologies Conference (PEDSTC), pp. 1-6, Feb. 2020

ISSN 2394 - 9554

[10] X. Li, Z. Deng, Z. Chen and Q. Fei, "Analysis and simplification of three-dimensional space vector PWM for three-phase four-leg inverters", IEEE Trans. Ind. Electron., vol. 58, no. 2, pp. 450-464, Feb. 2011

[11] Joao I. Y. Ota, Marcelo G. Villalva, Fujio Sato, Ernesto Ruppert. "3-D Space Vector PWM implementation for Four-Leg Voltage Source Inverter", XI Brazilian Power Electronics Conference, 2011

[12] P. Cortés, S. Kouro, B. La Rocca, R. Vargas and J. Rodríguez, "Guideline for weighting factors design in model predictive control of power converters and drives", Proc. IEEE Int. Conf. Ind. Technol., pp. 1-7, May 2009